

# Out-of-Time Ordered Correlators in Kicked Coupled Tops: Information Scrambling in Mixed Phase Space and the Role of Conserved Quantities

Naga Dileep Varikuti<sup>1,\*</sup> and Vaibhav Madhok<sup>1</sup>

<sup>1</sup>*Department of Physics, Indian Institute of Technology Madras, Chennai, India, 600036*

(Dated: August 30, 2023)

We investigate operator growth in a bipartite kicked coupled tops (KCT) system with out-of-time ordered correlators (OTOC). Due to the conservation of total magnetization, the system admits a decomposition into distinct invariant subspaces. Initially focusing on the largest invariant subspace, we observe that, under strong coupling, the OTOC growth rate correlates remarkably well with the classical Lyapunov exponent. For the case of scrambling in the mixed phase space, we invoke Percival's conjecture to partition the eigenstates of the Floquet map into regular and chaotic. We notice that the scrambling rate in the chaotic subspace is quantified by OTOCs calculated with respect to a random state constructed from the mixture of chaotic eigenstates described above. We then consider the total system and study OTOCs for different types of initial operators, including the case of random operators where the operators are chosen randomly from the Gaussian unitary ensemble. We observe that the presence of a conserved quantity results in different types of scrambling behaviors for various choices of initial operators depending on whether the operators commute with the symmetry operator. When the operators are random, the averaged OTOC is related to the linear entanglement entropy of the Floquet operator, as found in earlier works. More importantly, we derive a simple expression for the averaged OTOC when random operators commute with the symmetry operator. Our results offer (i) fresh insights into scrambling in mixed-phase space - a domain that has not been comprehensively explored before and (ii) implications of the conserved quantities on the scrambling of information.

## I. INTRODUCTION

Chaos in classical physics is closely related to non-integrability, ergodicity, complexity, entropy production, and thermalization, which are central to the study of many-body physics and classical statistical mechanics. The quantum mechanics of systems whose classical counterparts are chaotic, generally known as quantum chaos, aims to extend these ideas to the quantum domain. In classical physics, the sensitive dependence on initial conditions implies chaos. A naive generalization of classical chaos to the quantum domain fails due to the unitarity of quantum evolutions. Hence, it is necessary to find the signatures of chaos through various other means in quantum systems. Many quantities, such as level spacing statistics [1], entanglement entropy [2, 3], out-of-time ordered correlators (OTOCs) [4], and tri-partite mutual information [5], have emerged as powerful tools to characterize the chaos in quantum systems. OTOCs are particularly interesting due to their usefulness in characterizing various features of quantum many-body systems. Originally introduced in the theory of superconductivity [6], the OTOCs are being studied with renewed interest in the context of quantum many-body systems [7–11], quantum chaos [4, 5, 12–17], many-body localization [18–22] and holographic systems[23, 24]. The early time growth rate of OTOCs, in particular, is being actively studied[10, 13, 15, 25–38], which is a quantum counterpart of the classical Lyapunov exponent (LE).

In order to define the OTOC, consider two local Hermitian or unitary operators  $A$  and  $B$  acting on two disjoint local subsystems of a given system with the dimensions  $d_A$  and  $d_B$ , respectively. Then, a function of the commutator, namely the

squared commutator, is given by

$$C(t) = \frac{1}{2} \langle \psi | [A(t), B]^\dagger [A(t), B] | \psi \rangle, \quad (1)$$

where  $A(t) = U^\dagger(t)A(0)U(t)$  and  $U$  represents system's time evolution operator. For the sake of simplicity and experimental feasibility, the state  $|\psi\rangle$  is usually taken to be the maximally mixed state —  $\mathbb{1}/d_A d_B$ , where  $d_A$  and  $d_B$  denote subsystem dimensions. In this text, we consider Hermitian operators for OTOC calculations. Then, the commutator function becomes  $C(t) = C_2(t) - C_4(t)$ , where

$$C_2(t) = \frac{\text{Tr}(A^2(t)B^2)}{d_A d_B} \quad \text{and} \quad C_4(t) = \frac{\text{Tr}(A(t)BA(t)B)}{d_A d_B}. \quad (2)$$

Here,  $C_2(t)$  is a time-ordered two-point correlator, and  $C_4(t)$  represents the four-point correlator function.  $C_4(t)$  possesses an unusual time ordering, which is why it is referred to as OTOC (Out-of-Time-Ordered Correlator). The four-point correlator is the dominant factor driving the total commutator function  $C(t)$ . Hence, we use the terms OTOC and commutator function interchangeably to denote the same quantity  $C(t)$ .

In the semiclassical limit ( $\hbar \rightarrow 0$ ), the Poisson bracket replaces the commutator. For  $A = \hat{X}$  and  $B = \hat{P}$ , the semiclassical limit implies  $\{X(t), P\}^2 = (\delta X(t)/\delta X(0))^2 \sim e^{2\lambda t}$ , where  $\lambda$  denotes the maximum Lyapunov exponent (LE), which is positive for chaotic systems. The correspondence principle states that the dynamics of expectation values of observables in a quantum system follow corresponding classical equations of motion until a time known as Ehrenfest's time ( $t_{\text{EF}}$ ) that depends on the dynamics of the system. Hence, for the quantum systems whose classical analog is chaotic, one can expect that the OTOCs grow exponentially until the Ehrenfest time  $t_{\text{EF}}$  which scales with the system dimension (dim) and the LE as  $\sim \log(\text{dim})/\lambda$ . Though the early time growth rate

\* [vndileep@physics.iitmadras.ac.in](mailto:vndileep@physics.iitmadras.ac.in)

of OTOC correlates well with the LE for many chaotic systems, it is worthwhile to note that the exponential growth may not always represent chaos [39–43]. Moreover, in finite temperature systems, the growth rate is bounded by  $2\pi/\beta$  [4, 44]. For  $t > t_{\text{EF}}$ , quantum corrections (non-zero  $\hbar$ ) start dominating, resulting in the breakdown of the quantum-classical correspondence for the OTOC.

Recently, OTOCs have been found to have various interesting connections to other probes of quantum chaos such as spectral form factors [45], participation ratio [34], universal level statistics [37], operator entanglement entropy [46], tripartite mutual information [5], Loschmidt echo [35], frame potentials, and unitary designs [47]. OTOCs have also been investigated in systems with very few qubits and observed that the signatures of short-time exponential growth can still be found in such systems [48]. Another intriguing feature of OTOC is that in multipartite systems, the growth of OTOC is related to spreading an initially localized operator across the system degrees of freedom. The commutator-Poisson bracket connection gives an analog of the classical separation of two trajectories with quantum mechanical operators replacing the classical phase space trajectories. Under chaotic many-body dynamics, an initially simple local operator becomes increasingly complex and will have its support grown over many system degrees of freedom, thereby making the initially localized quantum information at later times hidden from the local measurements [5, 8, 15, 49]. As the operator evolves in the Heisenberg picture under chaotic dynamics, it will start to become incompatible with any other operator with which it commutes initially. Bi-partite systems are the simplest multipartite settings to study such a scenario. In this paper, we study the dynamics of OTOCs in the kicked coupled tops (KCT), a bipartite system with a well-defined classical limit. To this effect, a "coupled kicked tops" system has been previously studied [26] where two kicked tops that independently exhibit chaos were weakly coupled. In contrast, our system's mechanism of coupling and chaos is the same as we discuss in the next section.

This paper is structured as follows. In section II, we review some of the details of the KCT model. Section III is devoted to analyzing information scrambling in the KCT model. In section III A and III B, we examine scrambling in the largest subspace for the fully chaotic and mixed phase space regimes, respectively. In section III C and III D, we consider the entire system KCT system and study the scrambling for two different initial operator choices. Section IV is devoted to the cases of random operators, wherein we show that the OTOC for the random operators is connected to the operator entanglement and coherent generating power of the time evolution operator. Finally, we conclude the text in section V.

## II. MODEL: KICKED COUPLED TOP

The kicked coupled top (KCT) model, originally introduced in [50], is governed by the following Hamiltonian:

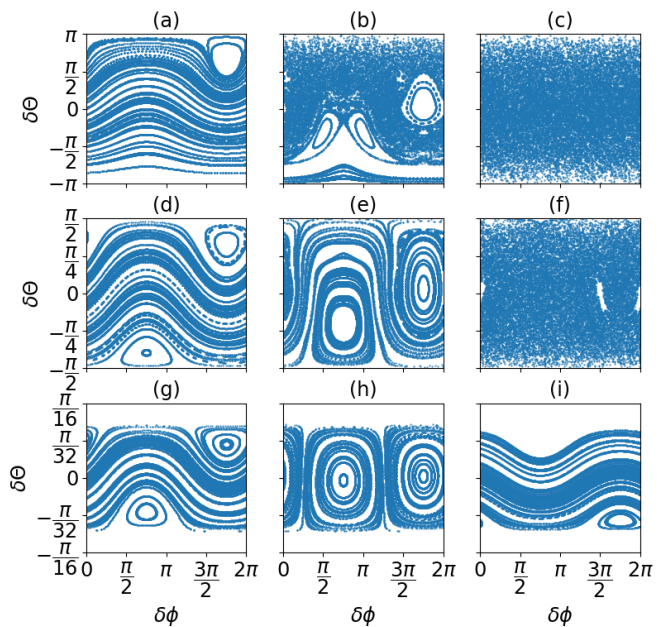


FIG. 1. Poincaré surface of sections corresponding to different coupling strengths (along the rows) and different sectors of  $F_z$  (along the columns). The kicking strength  $\beta$  is kept constant at  $\pi/2$ . Panels (a)-(c) illustrate the case where  $F_z/\sqrt{|\mathbf{I}||\mathbf{J}|} = 0$ . Along the row, the coupling strengths are  $\alpha = 1/2, 3/2$ , and 6 from left to right, respectively. In panels (d)-(f),  $F_z/\sqrt{|\mathbf{I}||\mathbf{J}|} = 1$ , while panels (g)-(i) illustrate  $F_z/\sqrt{|\mathbf{I}||\mathbf{J}|} = 1.99$ . For  $\alpha = 1/2$ , the phase space in the sectors close to  $F_z = 0$  remains mostly regular across all  $F_z$  sectors. However,  $\alpha = 3/2$  and  $\alpha = 6$  correspond to mixed and fully chaotic phase spaces. The phase space maintains regularity for all the couplings in the smaller sectors that are close to  $|F_z|/\sqrt{|\mathbf{I}||\mathbf{J}|} = 2$ .

$$H = \frac{\alpha}{\sqrt{|\mathbf{I}||\mathbf{J}|}} \mathbf{I} \cdot \mathbf{J} + \beta \sum_{n=-\infty}^{\infty} \delta(t - n\tau) J_z, \quad (3)$$

where  $\alpha$  and  $\beta$  denote coupling strength and kicking strength, respectively. For simplicity, we take  $|\mathbf{I}| = |\mathbf{J}| = J$ . The system evolution can be understood as alternating rotations of  $\mathbf{J}$  around  $z$ -axis, followed by a precession of  $\mathbf{I}$  and  $\mathbf{J}$  about the total angular momentum vector  $\mathbf{F} = \mathbf{I} + \mathbf{J}$  by an angle proportional to  $\alpha|\mathbf{F}|$ . Total magnetization along  $z$ -axis ( $F_z = \hat{I}_z + \hat{J}_z$ ) is the only known constant motion in this system. The absence of enough conserved quantities leads to non-integrability, resulting in chaotic behavior when  $\alpha$  is sufficiently large.

Phase space structures of the KCT model can be simulated using  $\text{SO}(3)$  matrices. Conservation of  $F_z$  allows the decomposition of the entire system into invariant sectors, each with a constant  $F_z$  value ranging from 0 to  $\pm 2J$ . The Poincaré surface sections corresponding to three different  $F_z$  sectors, namely,  $F_z = 0, 1$  and 1.99 are shown in Fig. (1) for a few different  $\alpha$  values. In the absence of coupling, the system remains integrable. As  $\alpha$  increases, the chaos slowly starts to build up, and for  $\alpha \geq 6$ , the system becomes fully chaotic in most of the  $F_z$  sectors. Fig. (2a) shows the illustration of maximum LE vs.  $\alpha$  calculated using Benettin's algorithm [51] in  $F_z = 0$  section. The plot suggests that the growth of the average Lyapunov exponent versus the coupling strength is logarithmic

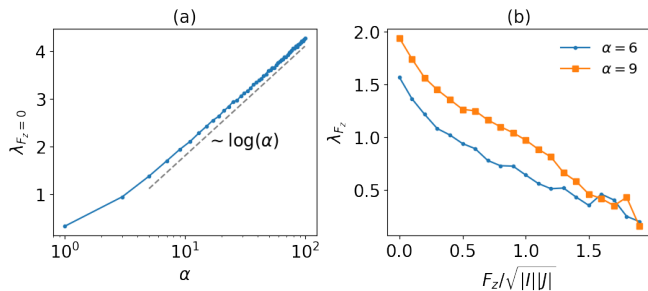


FIG. 2. (a) Illustration of the maximum Lyapunov exponent vs. coupling strength  $\alpha$  in the  $F_z = 0$  sector. At every  $\alpha$ , the exponent is averaged over  $10^3$  initial conditions. The plot suggests that the average Lyapunov exponent in the largest invariant subspace ( $\lambda_{F_z=0}$ ) follows an approximately logarithmic law. (b) The Lyapunov exponent is calculated for different values of  $F_z$ . The interaction strength and the kicking parameter are kept fixed at 6 and  $\pi/2$ , respectively.

—  $\lambda \sim \log(\alpha)$ . Interestingly, this is very similar to the analytical calculation of LE done for the kicked top in Ref. [52]. Moreover, as  $F_z$  increases, the area of the corresponding phase space sector decreases. As a result, the largest Lyapunov exponent  $\lambda_{F_z}$ , which roughly scales like  $\sim \log(\text{Area})$ , decreases. Fig. (2b) illustrates the maximum Lyapunov exponent ( $\lambda_{F_z}$ ) vs.  $F_z$  for a fixed  $\alpha$ . We observe that  $\lambda_{F_z}$  decreases linearly with  $F_z$ .

In the quantum regime, the evolution of the system is given by the following Floquet operator:

$$\hat{U} = \exp\left\{\frac{-i\alpha}{\sqrt{IJ}}\mathbf{I}\cdot\mathbf{J}\right\} \exp\{-i\beta\hat{J}_z\}, \quad (4)$$

where  $\mathbf{I}\cdot\mathbf{J} = \hat{I}_x\hat{J}_x + \hat{I}_y\hat{J}_y + \hat{I}_z\hat{J}_z$ . The quantum version of the KCT is also non-integrable due to insufficient conservation laws. In the uncoupled representation, the elements of  $\hat{U}$  can be written as follows:

$$U_{m_1 m_2, m_3 m_4} = \sum_{F=|M|}^{2J} e^{-i\frac{\alpha}{2\sqrt{|I||J|}}F(F+1)} e^{-i\beta m_4} C_{I, m_1; J, m_2}^{F, M} C_{I, m_3; J, m_4}^{F, M}, \quad (5)$$

where  $C_{I, m_i; J, m_j}^{F, M} = \langle F, M | I, m_i; J, m_j \rangle$  denote Clebsch-Gordan coefficients. Similar to its classical counterpart,  $\hat{U}$  also admits a decomposition into various invariant subspaces characterized by the quantum number  $F_z$  —  $U = \oplus_{F_z} U_{F_z}$ , where  $F_z$  runs from  $-2J$  to  $2J$ . As a result,  $U_{m_1 m_2, m_3 m_4} = 0$  whenever  $|m_1 + m_2| \neq |m_3 + m_4|$ . Moreover, the dimension of each subspace is related to  $F_z$  as  $d = 2J + 1 - |F_z|$ .

An interesting feature of quantum chaos is its connections with random matrix theory (RMT). As the KCT is a time-periodic system, the time evolution is governed by a Floquet unitary. Dyson introduced three random unitary ensembles [53], namely circular unitary ensemble (CUE), circular orthogonal ensemble (COE), and circular symplectic ensemble (CSE) based on their properties under time-reversal operation. If a system exhibits chaos in the classical limit ( $\hbar \rightarrow 0$ ), the spectral statistics of its evolution align with one of the three

random unitary ensembles. In the present case, we consider the generalized time-reversal operation and see that the system under study is invariant under the time-reversal operation.

$$T = e^{i\beta\hat{J}_z} K, \quad (6)$$

where  $K$  is complex conjugation in the uncoupled product basis. Since both  $\hat{I}_y$  and  $\hat{J}_y$  change sign under conjugation, while the  $x$  and  $z$  components of the angular momentum remain unaffected,

$$K\hat{J}_z K = \hat{J}_z; \quad K(\mathbf{I}\cdot\mathbf{J})K = \mathbf{I}\cdot\mathbf{J}. \quad (7)$$

Hence,

$$\begin{aligned} T U_\tau T^{-1} &= \left(e^{i\beta\hat{J}_z} K\right) \left(e^{-i\alpha\mathbf{I}\cdot\mathbf{J}} e^{-i\beta\hat{J}_z}\right) \left(K e^{-i\beta\hat{J}_z}\right) \\ &= e^{i\beta\hat{J}_z} \left(e^{i\alpha\mathbf{I}\cdot\mathbf{J}} e^{i\beta\hat{J}_z}\right) e^{-i\beta\hat{J}_z} \\ &= e^{i\beta\hat{J}_z} e^{i\alpha\mathbf{I}\cdot\mathbf{J}} = U_\tau^\dagger. \end{aligned} \quad (8)$$

As a result, the dynamics are invariant under time reversal operation. Moreover,  $T^2 = 1$ , hence there is no Kramer's degeneracy. Hence, COE is the appropriate unitary ensemble for the KCT model.

Significant efforts have been put into understanding the dynamics of the OTOCs in generic many-body quantum systems both in the presence and absence of conserved quantities. Conserved quantities have been shown to slow the information scrambling [54]. Moreover, the OTOCs will exhibit a diffusive relaxation if one of the operators has a non-zero overlap with the symmetry operator [9, 10]. The effect of conservation laws on scrambling has recently been studied in the context of holographic CFTs [55, 56]. Furthermore, if a many-body system with a conservation law follows the Eigenstate Thermalization Hypothesis (ETH), the OTOCs will exhibit algebraic relaxation towards the equilibrium value [57]. The works mentioned above investigated the dynamics of OTOCs in the context of many-body systems without obvious classical limits. However, there remains to be a gap in understanding the implications of conservation law on operator growth when the system has a smooth classical limit. Our work has two main goals: (i) Investigating operator growth dynamics for the time-reversal invariant KCT, which conserves total magnetization along the  $z$ -axis and (ii) Examining scrambling within the mixed-phase space.

### III. INFORMATION SCRAMBLING IN THE KCT MODEL

From the previous section, we observe that the KCT model conserves the total magnetization  $\hat{F}_z = \hat{I}_z + \hat{J}_z$ , i.e.,  $[\hat{U}, \hat{F}_z] = 0$ , leading to decomposition into invariant subspaces. In this system, scrambling is mainly driven by the largest subspace dynamics, but the near-integrable dynamics in smaller subspaces somewhat offset it. Classically, as one moves away from the  $F_z = 0$  sector, the corresponding area of the Poincaré section associated with each sector gradually decreases (see the Poincaré surface of sections in Fig. 1). In particular, near

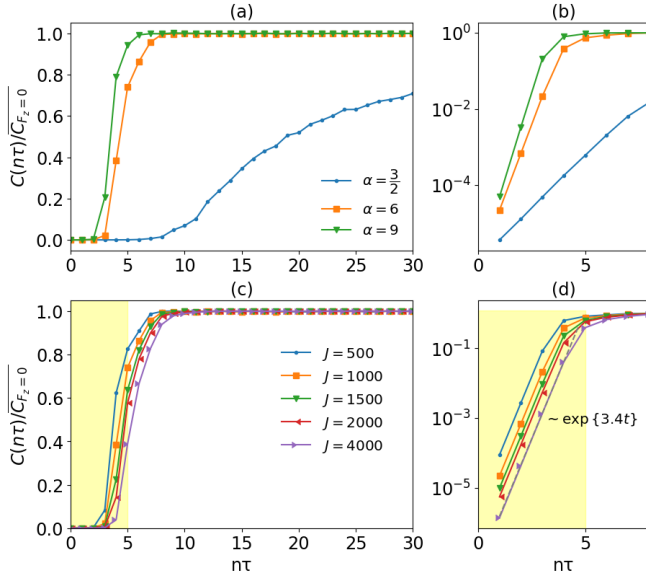


FIG. 3. (a) The figure illustrates OTOC growth in the largest subspace for three different couplings, with fixed  $J = 1000$ . In (b), corresponding early-time exponential growth is shown on a semi-log plot. Panels (c) and (d) demonstrate OTOC growth for a chaotic  $\alpha = 6$  for varying  $J$  values. The plots are normalized by plotting by dividing the OTOC with  $\overline{C_{F_z=0}}$ , the infinite time average of the OTOC.

$|F_z| = 2J$ , the area tends to vanish, leading to highly localized dynamics. This results in vanishingly small Lyapunov exponents —  $\lambda_{|F_z| \gg 0} \approx 0$  (see Fig. 2b). Accordingly, despite strong coupling, the corresponding quantum dynamics tend to become more regular. Therefore, we have regular dynamics for  $F_z$  close to  $\pm 2J$ , and the OTOC behavior is oscillatory. Hence, the OTOCs calculated within these subspaces do not show the characteristic short-time exponential growth and typically take longer to relax. As  $F_z$  is varied away from  $\pm 2J$ , the dynamics becomes non-integrable and eventually chaotic. In the following, we will begin by examining scrambling in the largest subspace, emphasizing OTOC dynamics in the chaotic and mixed phase space regimes. Afterward, we will analyze the OTOC dynamics for two pairs of initial operators, namely,  $(\hat{I}_z, \hat{J}_z)$  — where both operators commute with  $\hat{F}_z$ , and  $(\hat{I}_x, \hat{J}_x)$  — where neither operator commutes with the total magnetization  $\hat{F}_z$ .

### A. OTOC in the largest invariant subspace

Unlike smaller subspaces ( $|F_z| \gg 0$ ), at sufficiently strong coupling ( $\alpha \gtrsim 6$ ), the subspaces close to  $F_z = 0$  are predominantly chaotic. Here, we numerically study the OTOC for a pair of operators acting exclusively on the largest invariant subspace ( $F_z = 0$ ) of the KCT model. The corresponding Floquet

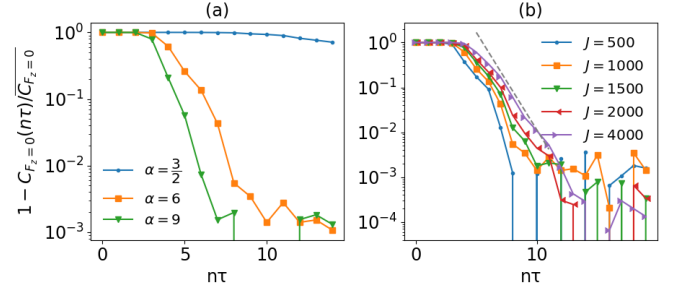


FIG. 4. Relaxation dynamics as probed by the quantity  $1 - C(n\tau)/\overline{C_{F_z=0}}$ . Panel (a) corresponds to the relaxation of the OTOC illustrated in Fig. 3a, and panel (b) shows the relaxation dynamics corresponding to Fig. 3c.

quet evolution, in the  $F_z = 0$ , can be written as follows:

$$\hat{U}_{F_z=0} = \sum_{F=0}^{2J} \sum_{m_1, m_2} e^{-i(\frac{\alpha}{2J}F(F+1) + \beta m_2)} C_{I, m_1; J, -m_1}^{F, 0} C_{I, m_2; J, -m_2}^{F, 0} |m_1\rangle \langle m_2|. \quad (9)$$

Here, the indices  $m_1$  and  $m_2$  run from  $-J$  to  $J$ , implying that the unitary acts on  $(2J + 1)$ -dimensional Hilbert space.

For the OTOC calculations, we take the initial operators  $A = B = \hat{S}_z$ . In the classical limit, for chaotic systems, the Ehrenfest time scales as  $t_{\text{EF}} \sim \log(\text{dim})/\lambda_{\text{cl}}$ . Within this timescale,  $C_{F_z=0}(t)$  shows exponential growth. The supporting numerical results are shown in Fig. 3. Figure 3a illustrates the operator growth for different values of  $\alpha$  by plotting the normalized OTOC —  $C_{F_z=0}(n\tau)/\overline{C_{F_z=0}}$  versus time. Here,  $\overline{C_{F_z=0}}$  denotes infinite time average of  $C_{F_z=0}(t)$  and is given by

$$\begin{aligned} \overline{C_{F_z=0}} &= \lim_{t \rightarrow \infty} \frac{1}{t} \int_0^t C_{F_z=0}(t) dt \\ &= \frac{1}{(2J+1)^2} \left[ \sum_m [A^2]_{mm} [B^2]_{mm} - [A_{mm}]^2 [B_{mm}]^2 \right. \\ &\quad \left. - \sum_{m \neq n} (A_{mm} A_{nn} B_{mm} B_{nn} + A_{mm} A_{nn} B_{nn} B_{mm}) \right], \quad (10) \end{aligned}$$

where  $A_{mm} = \langle E_m | A | E_m \rangle$  etc. and  $\hat{U}_{F_z=0} = \sum_n e^{-i\phi_n} |E_n\rangle \langle E_n|$  denotes the eigen-decomposition of the subspace Floquet operator. In the figure, the angular momentum is kept fixed at  $J = 1000$ . The figure shows that the growth rate increases with  $\alpha$ . Moreover, for  $\alpha = 3/2$ , the classical phase space has a mix of regular islands and the chaotic sea. This results in a slower OTOC growth than the fully chaotic cases, as illustrated in the figure 3a. We elaborate more on the mixed-phase space OTOC dynamics in the next subsection. Figure 3b demonstrates the corresponding early-time exponential growths of the OTOCs plotted in 3a. In Fig. 3c and 3d, we show the OTOC growth for the fully chaotic phase space for different dimensions by taking  $\alpha = 6$ . The corresponding numerical results yield a quantum exponent of  $\lambda_{\text{quant}} \approx 1.67$  for  $J = 4000$ , closely matching the classical LE,  $\lambda_{\text{cl}} \approx 1.55$ , indicating a good classical-quantum correspondence. A detailed presentation of the quantum exponents for different  $J$ -values is given in the table. I.

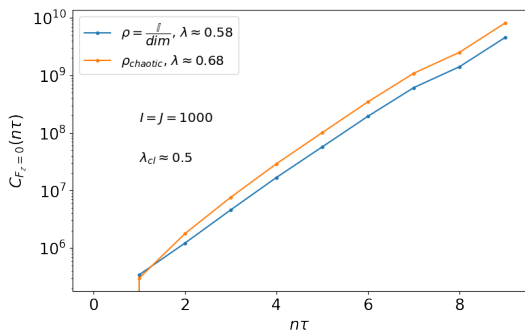


FIG. 5. Illustration of the OTOC growth when the system is associated with the mixed phase space in the classical phase space. We fix  $\alpha = 3/2$ ,  $\beta = \pi/2$  and  $J = 1000$ . In the figure, the blue curve represents the OTOC growth with respect to the maximally mixed state. The orange curve corresponds to the statistical mixture of the chaotic Floquet states:  $\rho_{\text{chaotic}} = \frac{1}{2J+1} \sum_{i=0}^k |E_i\rangle\langle E_i|$ , where  $\{|E_i\rangle\}_{i=0}^k$  represents a subset of chaotic Floquet states and  $k < 2J + 1$ . We have taken  $10^3$  chaotic Floquet states to construct  $\rho_{\text{chaotic}}$ .

A sharp relaxation to the saturation follows the initial growth. While the short-time behavior of the OTOCs is well-studied and understood, the relaxation is relatively unexplored, with only a few studies. For example, exponential relaxation has been found in random quantum circuit models [58] and maximally chaotic Floquet systems [59]. Relaxation in weakly coupled bipartite systems with chaotic subsystems has been studied in Ref. [26]. Given a localized state  $|\psi\rangle$  and a fully chaotic  $\hat{U}$ , randomization of the state implies that  $|\langle\psi|\hat{U}^t|\psi\rangle|^2 \sim e^{-\gamma t} \sim 1/(2J+1)$ . Then, the information gets fully scrambled in a time window of  $t_{\text{sc}} \sim \log(2J+1)/\gamma$ . Note that  $t_{\text{sc}}$  can not be smaller than  $t_{\text{EF}}$ , i.e.,  $t_{\text{EF}} \lesssim t_{\text{sc}}$ . Therefore, in strongly chaotic systems, the relaxation takes place over a window of time  $t_{\text{relx}} = (t_{\text{sc}} - t_{\text{EF}}) \sim \log(2J+1)$ . Beyond this, we expect that the OTOC will get saturated. To study the relaxation, we take the quantity  $1 - C_{F_z=0}(n\tau)/\overline{C_{F_z=0}}$ . The relaxation dynamics are illustrated in Fig. 4. While Fig. 4a demonstrates the decay of  $1 - C_{F_z=0}(n\tau)/\overline{C_{F_z=0}}$  for a few different  $\alpha$  values, Fig. 4b illustrates that same for different  $J$  values while keeping  $\alpha$  fixed. In the fully chaotic regime, we observe that the relaxation follows an exponential decay. The figure also confirms the logarithmic scaling of the relaxation time with the Hilbert space dimension. For instance,  $t_{\text{relx}}(J_1=4000)/t_{\text{relx}}(J_2=500) \approx 1.6$ , which closely matches  $\log(2J_1+1)/\log(2J_2+1) \approx 1.3$ . Though not the central focus of our work, we find the relaxation dynamics an interesting observation subject to further exploration.

### B. Scrambling in the mixed phase space $\left(\alpha = \frac{3}{2}, \beta = \frac{\pi}{2}\right)$

If the system is fully chaotic, the OTOC reaches a saturation point followed by the initial exponential growth and relaxation. However, an interesting scenario appears if the classical limit of the system lies in a mixed phase space. To be specific, the initial states with a substantial overlap with

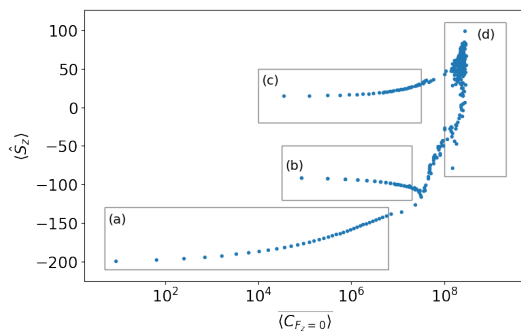


FIG. 6. Illustration of  $\langle \hat{S}_z \rangle$  versus long-time averaged OTOC for the Floquet states associated with the mixed phase space of the KCT model ( $\alpha = 3/2$  and  $\beta = \pi/2$ ) in the largest subspace. Boxes (a), (b), and (c) correspond to the Floquet states localized on the regular regions of the phase space. Box (d) represents a series of chaotic states, that display flat  $\overline{C_{F_z=0}}$ . The angular momentum value is taken to be  $I = J = 200$

the coherent states centered around stable fixed points limit the degree of scrambling. To see this, we first consider an initial state, which is an arbitrary mixture of coherent states whose mean coordinates are located on the chaotic sea. Such states can be realized by invoking Percival's conjecture [60]. The conjecture categorizes Eigenstates or Floquet states of the system into regular (near stable fixed points) and chaotic states (randomly distributed across chaotic regions). Yet, it's important to note that Percival's conjecture is not always accurate, particularly in the deep quantum regime. Nevertheless, quantities such as Husimi entropy of the states can be employed to roughly distinguish the regular states from the chaotic ones [50]. As chaotic Floquet states are widespread across the chaotic sea, we choose a random mixture of a handful of such states instead of infinitely many coherent states. After initializing the system in such a mixture of states, we compute the largest subspace OTOC by fixing the initial operators  $A = B = \hat{S}_z$ . The corresponding results are shown in Fig. 5. The figure compares the OTOC growth in the mixture of chaotic states with that of the maximally mixed state. While the former shows a growth rate of  $\lambda_\rho \approx 0.68$ , the latter grows at a slightly lesser rate given by  $\lambda_{1/\dim} \approx 0.58$ . The slight difference in the growth rates highlights that the chaotic states enhance the scrambling of information. On the contrary, the regularity of the states centered near the regular islands causes a slowdown of the scrambling.

We now elucidate the role of Percival's conjecture in the saturation of mixed phase space OTOC. To do so, we calculate infinite time averages of the OTOC in the Floquet states and contrast the regular states with the chaotic states:

$$\overline{\langle E_n | C_{F_z=0} | E_n \rangle} = \lim_{t \rightarrow \infty} \frac{1}{t} \int_0^t ds \langle E_n | [A(s), B]^\dagger [A(s), B] | E_n \rangle. \quad (11)$$

A comparison between the chaotic and the regular states can be drawn by plotting  $\overline{\langle E_n | C_{F_z=0} | E_n \rangle}$  versus the mean location of  $|E_n\rangle$  on the phase space. The mean location can be identified by finding  $\langle E_n | \hat{S}_z | E_n \rangle$ , which correlates to  $\delta\theta$  in the semiclassical limit. Figure 6 shows  $\overline{\langle E_n | C_{F_z=0} | E_n \rangle}$  vs.  $\langle E_n | \hat{S}_z | E_n \rangle$

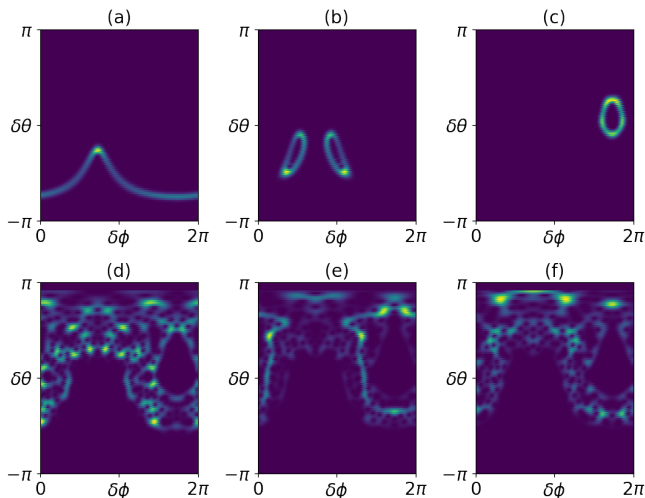


FIG. 7. Husimi distributions of the Floquet states of  $\hat{U}_{F_z=0}$ . The system parameters correspond to the mixed phase space in the classical limit —  $\alpha = 3/2$  and  $\beta = \pi/2$ . The Floquet states in (a), (b), and (c) are chosen randomly from the series of points inside the boxes (a), (b), and (c) respectively in Fig. 6. These three states are localized around different fixed points. (d)-(f) panels correspond to the chaotic Floquet states randomly chosen from the box 6d.

for a fixed  $J = 200$  and  $\alpha = 3/2$ . The correlation between  $\langle \hat{S}_z \rangle$  and  $\delta\theta$  causes Floquet states near stable fixed points to display identical  $\langle \hat{S}_z \rangle$  values [50, 61]. In the figure, box (a) corresponds to the series of states localized near the stable south pole [see Fig. 7a]. The boxes (b) and (c) correspond to the regular islands displayed in Fig. 7b and Fig. 7c. Moreover, the chaotic Floquet states typically saturate the value of  $\langle E_n | C_{F_z=0} | E_n \rangle$  as they are delocalized in the chaotic sea. These states are concentrated vertically along a line within box (d). Husimi plots of three randomly chosen chaotic Floquet states are shown in Fig. 7d-7f. Lesser values of the time-averaged OTOC for the states chosen from boxes (a), (b), and (c) indicate that the operators are less prone to get scrambled if the initial state is localized on a regular island.

For completeness, we also compute infinite time averages of the OTOC using coherent states as initial states:  $\langle \delta\theta, \delta\phi | C_{F_z=0} | \delta\theta, \delta\phi \rangle$ . We focus on correlating these averages with the classical phase space. The quantum signatures of the classical phase space structures appear in various contexts, including the dynamical generation of entanglement [2, 50, 62–65], tri-partite mutual information [12], quantum discord [66] and information gain in quantum state tomography [67, 68]. To proceed, we consider tensor products of spin coherent states  $|\theta_I, \phi_I\rangle \otimes |\theta_J, \phi_J\rangle$  and project them onto the  $F_z = 0$  subspace:

$$|\delta\theta, \delta\phi\rangle = \frac{1}{\mathcal{N}} \sum_{m=-J}^J \mu^m \frac{(2J)!}{(J-m)!(J+m)!} |m, -m\rangle, \quad (12)$$

where

$$\mu = e^{i\delta\phi/2} \left( \frac{1 + \sin(\delta\theta/2)}{1 - \sin(\delta\theta/2)} \right)$$

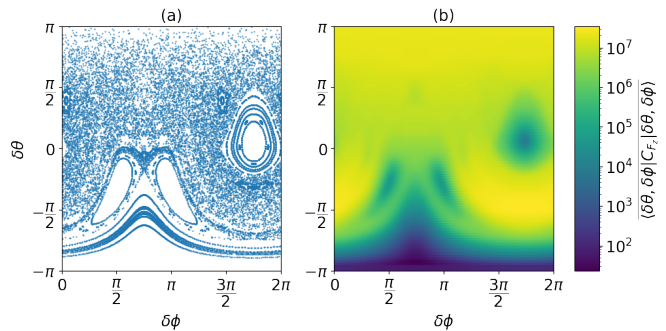


FIG. 8. (a) and (b). Side-by-side comparison, showing the infinite-time average of the largest subspace OTOC in the spin coherent states (Fig. (b)) as a superb signature of classical chaos in mixed-phase space ( $\alpha = 3/2, \beta = \pi/2$ ) as shown by the Poincaré surface of the section in (a). The angular momentum value is taken to be  $I = J = 100$ .

$\alpha = 6, \beta = \pi/2$			
Dimension	$\lambda_{F_z=0}$	$\lambda_{I_z, J_z}$	$\lambda_{cl(F_z=0)}$
$J=500$	$1.7108 \pm O(10^{-4})$ $t_{EF} \approx 4$	$1.47 \pm O(10^{-2})$ $t_{exp} \approx 4$	$\approx 1.55$
$J=1000$	$1.7246 \pm O(10^{-4})$ $t_{EF} \approx 4$	$1.362 \pm O(10^{-2})$ $t_{exp} \approx 4$	
$J=2000$	$1.6406 \pm O(10^{-3})$ $t_{EF} \approx 5$		
$J=4000$	$1.6988 \pm O(10^{-3})$ $t_{EF} \approx 5$		

TABLE I. The table illustrates the classical Lyapunov exponent of the largest subspace ( $\lambda_{cl(F_z=0)}$ ) and contrasts it with the OTOC growth rate in the largest subspace ( $\lambda_{F_z=0}$ ) for different  $J$ -values. Further contrast is made between  $\lambda_{F_z=0}$  and the growth rate of  $C_{I_z, J_z}(t)$ , which is denoted by  $\lambda_{I_z, J_z}$ . We fix the parameters of the system at  $\alpha = 6$  and  $\beta = \pi/2$ . Closeness of  $\lambda_{F_z=0}$  and  $\lambda_{cl(F_z=0)}$  indicates good quantum-classical correspondence. Moreover, we observe that  $\lambda_{I_z, J_z}$  is always slightly less than  $\lambda_{F_z=0}$  (see the main text for more details).

and  $\mathcal{N}$  denotes normalizing constant. We now replace the Floquet states  $\{|E_n\rangle\}$  with the coherent states in the Eq. (11). Fig. 8a and 8b shows the side-by-side comparison between the classical Poincaré section and the scatter plot of the infinite time averaged OTOC (unnormalized) in a mixed-phase space ( $\alpha = 3/2$ ). We see a remarkable correlation between the classical phase space and  $\langle \delta\theta, \delta\phi | C_{F_z=0} | \delta\theta, \delta\phi \rangle$ . We see that the latter reproduces classical phase space structures, such as regular islands and the chaotic sea. The operators are more likely to get scrambled in states that are centered in chaotic regions. On the other hand, the darker regions encircle stable fixed points where the operators remain stable and less prone to scrambling.

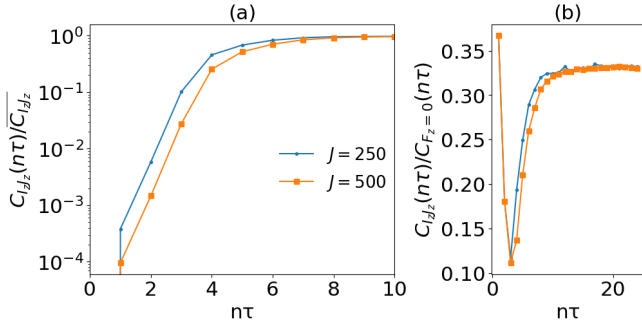


FIG. 9. (a) Illustration of the early-time exponential growth of  $C_{\hat{I}_z \hat{J}_z}(n\tau)/\overline{C_{\hat{I}_z \hat{J}_z}}$  for two different  $J$  values. The initial operators are  $A = \hat{I}_z \otimes \mathbb{I}$  and  $B = \mathbb{I} \otimes \hat{J}_z$ . Here,  $\alpha$  is kept fixed at 6. (b)  $C_{\hat{I}_z \hat{J}_z}(n\tau)/C_{F_z=0}(n\tau)$  vs.  $n\tau$  for the same  $J$  values as before, which aims to elucidate the influence of the largest subspace dynamics on the overall OTOC dynamics

### C. The $\hat{I}_z \hat{J}_z$ OTOC

Here, we compute the OTOC for the entire system of KCT by considering the initial operators  $A = \hat{I}_z \otimes \mathbb{I}$  and  $B = \mathbb{I} \otimes \hat{J}_z$ . Since  $A$  and  $B$  commute with  $F_z$ , they can be decomposed as  $A = \oplus_{F_z} A_{F_z}$ , and  $B = \oplus_{F_z} B_{F_z}$ . Accordingly, the commutator function  $C(t)$  becomes

$$C_{\hat{I}_z \hat{J}_z}(t) = \frac{1}{(2J+1)^2} \sum_{F_z} \text{Tr}[A_{F_z}^2(t) B_{F_z}^2] - \text{Tr}[A_{F_z}(t) B_{F_z} A_{F_z}(t) B_{F_z}] \quad (13)$$

where  $A_{F_z}(t) = U_{F_z}^\dagger A_{F_z} U_{F_z}$ . Given the absence of cross-terms between different subspaces, each subspace makes an independent contribution to the OTOC. We shall see from the numerical results that  $C_{\hat{I}_z \hat{J}_z}(t)$  shows a growth rate slightly less than that of  $C_{F_z=0}(t)$  over a short period. This can be intuitively understood by examining the following quantity:

$$\frac{C_{\hat{I}_z \hat{J}_z}(t)}{C_{F_z=0}(t)} = \frac{1}{2J+1} \left[ 1 + \sum_{\substack{F_z=-2J \\ F_z \neq 0}}^{2J} \left( 1 - \frac{|F_z|}{2J+1} \right) \frac{C_{F_z}(t)}{C_{F_z=0}(t)} \right], \quad (14)$$

where  $C_{F_z}(t)$  denotes OTOC contribution from a subspace with quantum number  $F_z$ . Due to the fully chaotic nature, the largest subspace will likely have the shortest Ehrenfest time. For  $t \lesssim t_{\text{EF}(F_z=0)}$ , there is a high chance that in the subspaces close to the largest one, the OTOCs will grow exponentially with the rates  $\lambda_{F_z \neq 0} \approx \lambda_{F_z=0}$ . Consequently,  $C_{F_z \neq 0}(t)/C_{F_z=0}(t) \sim \exp\{2(\lambda_{F_z \neq 0} - \lambda_{F_z=0})t\}$  either decays exponentially but slowly or stays a constant. On the other hand, for  $|F_z| \gg 0$ , the quantity  $C_{F_z \neq 0}(t)/C_{F_z=0}(t)$  decays quickly to zero. Therefore,  $C_{\hat{I}_z \hat{J}_z}(t)/C_{F_z=0}(t)$  most likely decays for  $t \lesssim t_{\text{EF}(F_z=0)}$ . As a result, the initial growth rate of  $C_{\hat{I}_z \hat{J}_z}(t)$  is expected to be slightly lower than that of  $C_{F_z=0}(t)$ . We confirm this from the numerical simulations shown in Fig. 9. For the numerical simulations, we consider  $\alpha = 6$ , which is strong enough to make a large number of subspaces fully chaotic.

In Fig. 9a, we plot the short-time exponential growth of the OTOC for two different  $J$  values. The plot is normalized by

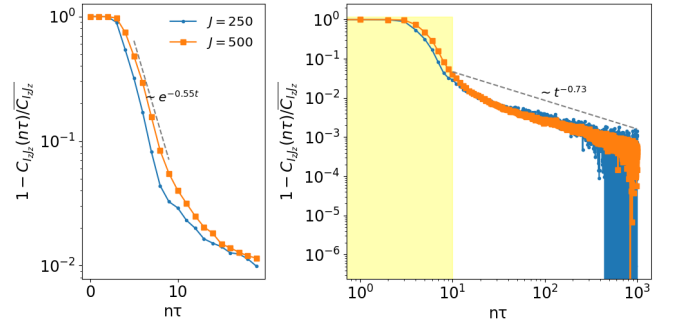


FIG. 10. Illustration of the two step relaxation of the  $\hat{I}_z - \hat{J}_z$  OTOC. (a) short-time exponential decay of  $1 - C_{\hat{I}_z \hat{J}_z}(n\tau)/\overline{C_{\hat{I}_z \hat{J}_z}}$ . The largest subspace dynamics largely dominate this phase. (b). Long-time algebraic decay of  $1 - C_{\hat{I}_z \hat{J}_z}(n\tau)/\overline{C_{\hat{I}_z \hat{J}_z}}$  in the second-phase.

dividing  $C_{\hat{I}_z \hat{J}_z}(t)$  with its infinite time average. Table. I makes a comparison between  $\lambda_{\hat{I}_z \hat{J}_z}$  and  $\lambda_{F_z=0}$ , and we see that the former is always slightly less than the latter, as inferred earlier. The quantity  $C_{\hat{I}_z \hat{J}_z}(t)/C_{F_z=0}(t)$  is examined for  $t \geq 1$  in Fig. 9b. The ratio initially decays with time for  $1 \leq t \leq 3$ , indicating that the largest subspace dominates. The decay time scale correlates with  $t_{\text{EF}(F_z=0)}$ . The ratio will grow afterward until the saturation, suggesting non-trivial contributions from the other subspaces.

We now study the relaxation dynamics using the quantity  $1 - C_{\hat{I}_z \hat{J}_z}(n\tau)/\overline{C_{\hat{I}_z \hat{J}_z}}$ . Recall that the subspace dynamics transition from chaotic to regular as  $|F_z|$  is increased from zero. Consequently, we observe (i) longer Ehrenfest times with slower growth rates and (ii) lesser saturation values as predicted by RMT in those subspaces. Due to the observations (i) and (ii),  $C_{\hat{I}_z \hat{J}_z}(t)$  takes a longer time to saturate compared to  $C_{F_z=0}(t)$ . The numerical results are shown in Fig. 10. The relaxation, as the figure suggests, proceeds in two steps. The first phase (see Fig. 10a), which is considerably dominated by the largest subspace dynamics, displays an exponential decay. The decay exponent correlates with that of  $1 - C_{F_z=0}(t)/C_{F_z=0}$ . For  $J = 500$ , the decay exponent is obtained to be  $\approx 0.55$ . At the end of this phase, the OTOC contributions from the subspaces close to  $F_z = 0$  almost reach a saturation point. The relaxation then shows a crossover to an algebraic law  $\sim t^{-0.73}$ , where the smaller subspace dynamics dominate. Moreover, due to the regular dynamics of those subspaces, we observe large fluctuations in the quantity  $1 - C_{\hat{I}_z \hat{J}_z}(t)/\overline{C_{\hat{I}_z \hat{J}_z}}$  as  $t$  approaches infinity. As  $\alpha$  increases further, smaller subspaces eventually become chaotic, leading to sharper decay in the first phase and flatter dynamics in the second phase.

### D. The $\hat{I}_x \hat{J}_x$ OTOC

Here, we study the operator growth for the local operators that do not commute with  $\hat{F}_z$ . Specifically, we take  $A = \hat{I}_x \otimes \mathbb{I}$  and  $B = \mathbb{I} \otimes \hat{J}_x$ . Unlike  $\hat{I}_z$  and  $\hat{J}_z$ , these operators do not admit the decomposition into disjoint invariant subspaces. Thus, OTOC dynamics are mixed across various subspaces. We aim

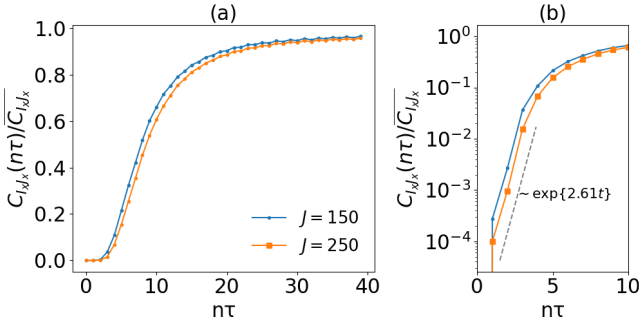


FIG. 11. (a) The OTOC when the initial operators are  $A = \hat{I}_x \otimes \mathbb{I}$  and  $B = \mathbb{I} \otimes \hat{J}_x$  for two different  $J$  values. The parameters are kept fixed at  $\alpha = 6$  and  $\beta = \pi/2$ . (b) Illustration of the early-time exponential growth on the semi-log scale.

to contrast the scrambling in this case with the previous one. First, for the initial operators  $A$  and  $B$ , it is useful to note that the following:

$$\left. \begin{aligned} \hat{U}_{F_z}^\dagger A \hat{U}_{F_z}^\dagger \neq 0 \\ \hat{U}_{F_z}^\dagger B \hat{U}_{F_z}^\dagger \neq 0 \end{aligned} \right\} \text{iff } F'_z = F_z \pm 1, \quad (15)$$

where  $\hat{U}_{F_z}$  remains  $(2J + 1)^2$ -dimensional, but acts non-trivially on the  $F_z$ -subspace alone. We again emphasize that the  $F_z = 0$  subspace typically drives the overall OTOC dynamics. However, the observation in Eq. (15) results in vanishing 4-point correlators at all the subspace levels, i.e.,

$$\text{Tr} \left[ \hat{U}_{F_z}^{\dagger t} A \hat{U}_{F_z}^\dagger B \hat{U}_{F_z}^{\dagger t} A \hat{U}_{F_z}^\dagger B \right] = 0 \quad \forall F_z \text{ and } t \geq 0. \quad (16)$$

On the contrary, the 4-point correlators that connect adjacent subspaces as given by  $\text{Tr} \left[ \hat{U}_{F_z}^{\dagger t} A \hat{U}_{F_z \pm 1}^\dagger B \hat{U}_{F_z}^{\dagger t} A \hat{U}_{F_z \pm 1}^\dagger B \right]$  remain non-vanishing. The intertwining of adjacent subspace evolutions  $\hat{U}_{F_z}$  and  $\hat{U}_{F_z \pm 1}$  causes slow down of the OTOC dynamics whenever the largest subspace is supposedly dominant.

We now numerically calculate  $C_{\hat{I}_x, \hat{J}_x}(n\tau)$  for two different values of  $J$ , namely,  $J = 150$  and  $J = 250$ . The corresponding results are plotted in Fig. 12. Figure 12a demonstrates growth of  $C_{\hat{I}_x, \hat{J}_x}(n\tau)/C_{\hat{I}_x, \hat{J}_x}$  and the corresponding short-time exponential growth is depicted in Fig. 12b. The parameters  $\alpha$  and  $\beta$  are kept fixed at 6 and  $\pi/2$ , respectively, as before. The exponential growth appears within the regime  $1 \leq t \leq 3$  for both values of  $J$ . Through the exponential fitting, we find  $\lambda_{\hat{I}_x, \hat{J}_x}(J=150) \approx 1.305$  and  $\lambda_{\hat{I}_x, \hat{J}_x}(J=250) \approx 1.388$ , which are roughly about the same as those of  $\lambda_{\hat{I}_z, \hat{J}_z}$ , but with a minute difference (see Table. I). However, the OTOC displays slower relaxation in the intermediate regime than in the previous case. For instance, for  $J = 250$ , we observe  $(1 - C_{\hat{I}_x, \hat{J}_x}(t)/C_{\hat{I}_x, \hat{J}_x}) \sim \exp\{-0.15t\}$ , which is in contrast with the previous case, where  $(1 - C_{\hat{I}_z, \hat{J}_z}(t)/C_{\hat{I}_z, \hat{J}_z}) \sim \exp\{-0.6t\}$ . Hence, the above inference about the slowdown of OTOC dynamics is justified.

Beyond the exponential decay, the quantity  $1 - C_{\hat{I}_x, \hat{J}_x}(t)/C_{\hat{I}_x, \hat{J}_x}$  displays a crossover to an algebraic law. For  $J=250$ , through the power law fitting of the data in this regime, we find that the

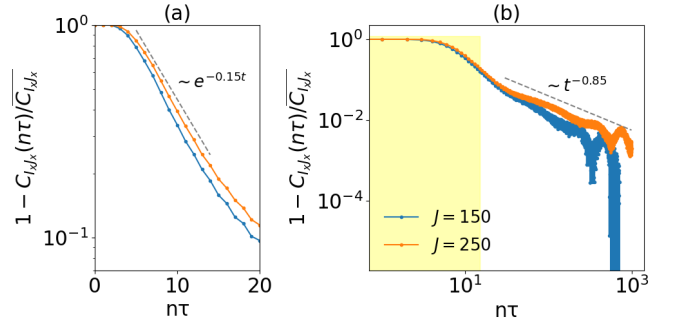


FIG. 12. Relaxation dynamics of the  $I_z - J_z$  OTOC. In (a), the short-time exponential decay of  $1 - C_{\hat{I}_x, \hat{J}_x}(n\tau)/C_{\hat{I}_x, \hat{J}_x}$  is shown, which is slower than its  $I_z - J_z$  counterpart (see text). (b). Long-time relaxation following algebraic decay  $\sim t^{-1.065}$  and  $\sim t^{-0.85}$  respectively for  $J = 150$  and  $J = 250$ .

relaxation follows an approximate scaling  $\sim t^{-0.85}$ , which is slightly faster than the earlier case of  $1 - C_{\hat{I}_z, \hat{J}_z}(t)/C_{\hat{I}_z, \hat{J}_z} \sim t^{-0.75}$ . Moreover, due to the regular dynamics associated with the smaller subspaces of the KCT model, the saturation is usually accompanied by fluctuations around the mean value of the OTOC.

We now evaluate  $C_{\text{RMT}}$  for the given operators  $A$  and  $B$ . To obtain the random matrix value of the OTOC, we replace the Floquet operator  $\hat{U}$  of the KCT model in the OTOC with  $\hat{V} = \oplus_{F_z} \hat{V}_{F_z}$ , where  $\hat{V} \in \text{CUE}(2J + 1 - |F_z|)$ , which is followed by the ensemble average. The observation in Eq. (15) assists in simplifying the COE average of the two-point and four-point correlators as follows:

$$\begin{aligned} \overline{C_2} &= \frac{1}{(2J + 1)^2} \sum_{F_z} \text{Tr} \left[ \overline{\hat{U}_{F_z}^\dagger A^2 \hat{U}_{F_z} B^2} \right] \\ &= \frac{1}{(2J + 1)^2} \sum_{F_z} \frac{\text{Tr}([A^2]_{F_z}^T B^2) + \text{Tr}([A^2]_{F_z}) \text{Tr}([B^2]_{F_z})}{2J + 2 - |F_z|} \end{aligned} \quad (17)$$

and

$$\begin{aligned} \overline{C_4} &= \frac{1}{(2J + 1)^2} \sum_{F_z} \text{Tr} \left[ \overline{\hat{U}_{F_z}^\dagger A \hat{U}_{F_z \pm 1} B \hat{U}_{F_z}^\dagger A \hat{U}_{F_z \pm 1} B} \right] \\ &= 0, \end{aligned} \quad (18)$$

where  $[A^2]_{F_z} = \mathbb{I}_{F_z} A^2 \mathbb{I}_{F_z}$  and  $\mathbb{I}_{F_z}$  is an identity operator acting exclusively on the  $F_z$ -subspace, i.e.,  $\mathbb{I}_{F_z} \equiv \mathbb{I}_{F_z} \oplus \mathbb{O}_{\text{rest}}$ , the null matrix  $\mathbb{O}_{\text{rest}}$  acts on rest of the subspaces. It then follows that  $C_{\text{RMT}} = \overline{C_2}$ .

#### IV. SCRAMBLING, OPERATOR ENTANGLEMENT AND COHERENCE

The previous section has been devoted to the OTOCs for the initial operators having smooth classical limits. Now, we focus on the random Hermitian operators taken from the unitarily invariant Gaussian ensemble (GUE). In this case, the

OTOCs lack an initial Lyapunov phase due to the inherent randomness of the operators with no obvious classical limits. In bipartite quantum systems, the OTOCs have a connection with the linear operator entanglement entropy of the system evolution when the initial operators are local Haar random unitaries [5, 46]. In this section, we show that the relationship persists for the GUE operators as well. Additionally, for the diagonal GUE matrices, we find that the OTOCs are related to the coherence-generating power introduced in Ref. [69].

### A. GUE initial operators

Given an arbitrary bipartite unitary  $U$ , we are interested in calculating the OTOC for two initial operators  $A = O_1 \otimes \mathbb{I}$  and  $B = \mathbb{I} \otimes O_2$ , where  $O_1 \in \text{GUE}(d_1)$  and  $O_2 \in \text{GUE}(d_2)$ . For simplicity, we take  $d_1 = d_2$ . Then, by averaging out these operators over GUE, the OTOC can be obtained as a function of the dynamics alone. By noting that the GUE is unitary invariant, we obtain the following:

$$\begin{aligned} \int_O O^2 dO &= \int_O dO \int_{u \in U(d)} duu^\dagger O^2 u \\ &= \frac{1}{d} \int_O dO \text{Tr}(O^2) \mathbb{I} \\ &= d \mathbb{I}_d, \end{aligned} \quad (19)$$

where in the third equality, we substituted  $\int \text{Tr}(O^2) = d^2$  and  $d$  denotes dimension of the operator  $O$ . We then obtain

$$\overline{C_2}(t) = \text{Tr} \left[ \hat{U}^{\dagger t} \left( \int dO_1 O_1^2 \right) \hat{U}^t \left( \int dO_2 O_2^2 \right) \right]. \quad (20)$$

From Eq. (19), we get  $\overline{C_2}(t) = d^4$ . We now consider the four-point correlator:

$$\begin{aligned} C_4(t) &= \text{Tr} \left[ \hat{U}^{\dagger t} O_1 \hat{U}^t O_2 \hat{U}^{\dagger t} O_1 \hat{U}^t O_2 \right] \\ &= \text{Tr} \left[ S \hat{U}^{\dagger \otimes 2} \{O_1 \otimes O_1\} \hat{U}^{t \otimes 2} \{O_2 \otimes O_2\} \right]. \end{aligned} \quad (21)$$

Similar to Eq. (19), by utilizing the unitary invariance of the GUE again, we get

$$\int_O (O \otimes O) dO = \int_O dO \int_{u \in U(d)} duu^{\dagger \otimes 2} O^{\otimes 2} u^{\otimes 2}. \quad (22)$$

The second integral can be solved as follows:

$$\begin{aligned} \int_{u \in U(d)} duu^{\dagger \otimes 2} O^{\otimes 2} u^{\otimes 2} &= \left( \left[ \frac{\text{Tr}(O)^2}{d^2 - 1} - \frac{\text{Tr}(O^2)}{d(d^2 - 1)} \right] \mathbb{I}_{d^2} \right. \\ &\quad \left. - \left[ \frac{\text{Tr}(O)^2}{d(d^2 - 1)} - \frac{\text{Tr}(O^2)}{d^2 - 1} \right] S \right) \end{aligned} \quad (23)$$

where  $S$  swaps the quantum states between the Hilbert space  $\mathcal{H}_{1(2)}$  and its replica. It then follows that

$$\int_O (O \otimes O) = S, \quad (24)$$

where we made the following substitutions:

$$\begin{aligned} \int_O dO \text{Tr}(O)^2 &= d \\ \int_O dO \text{Tr}(O^2) &= d^2. \end{aligned} \quad (25)$$

Accordingly, upon averaging over the local GUE matrices, the four-point correlator becomes

$$\overline{C_4}(t) = \text{Tr} \left[ S_{11} (\hat{U}^{\dagger t})^{\otimes 2} S_{11} (\hat{U}^t)^{\otimes 2} \right]. \quad (26)$$

It then follows that

$$C_{\text{GUE}}(t) = \frac{1}{d^2} \left[ d^4 - \text{Tr} \left[ S_{11} (\hat{U}^{\dagger t})^{\otimes 2} S_{11} (\hat{U}^t)^{\otimes 2} \right] \right], \quad (27)$$

where the second term is related to the linear entanglement entropy of quantum evolutions [46].

### B. Random diagonal initial operators

Here, the initial operators are  $A = O_1 \times \mathbb{I}$  and  $B = \mathbb{I} \otimes O_2$  and we take  $O_1$  and  $O_2$  to be Gaussian diagonal operators. These operators naturally commute with the total magnetization operator  $\hat{F}_z$ .

$$O_1 = \sum_{i=0}^{d-1} x_i |i\rangle \langle i| \quad \text{and} \quad O_2 = \sum_{i=0}^{d-1} y_i |i\rangle \langle i|, \quad (28)$$

where  $x_i$  and  $y_i$  are independent Gaussian random variables. It then follows that

$$\begin{aligned} \int_{O_{1(2)}} O_{1(2)}^2 dO_{1(2)} &= \mathbb{I}_{1(2)}, \\ \text{and} \quad \int_{O_{1(2)}} (O_{1(2)} \otimes O_{1(2)}) dO_{1(2)} &= \sum_{i,j=0}^{d-1} \delta_{ij} |i\rangle \langle i| |j\rangle \langle j|. \end{aligned} \quad (29)$$

Since the operators  $A$  and  $B$  commute with  $F_z$ , the computations can be done for each subspace separately. Therefore,

$$\begin{aligned} \overline{C_2}(t) &= d^2 \\ \overline{C_4}(t) &= \sum_{F_z} \sum_{ijkl} \langle ji | U_{F_z}^{\dagger \otimes 2}(t) |kk\rangle \langle kk | U_{F_z}^{\otimes 2}(t) |ll\rangle \delta_{il} \delta_{lj} \\ &= \sum_{F_z} \sum_{kl} \langle kk | \hat{U}_{F_z}^{\otimes 2}(t) |ll\rangle \langle ll | \hat{U}_{F_z}^{\dagger \otimes 2}(t) |kk\rangle \\ &= \sum_{F_z} \sum_{kl} |\langle k | \hat{U}_{F_z}(t) |l\rangle|^4 \end{aligned} \quad (30)$$

Hence the commutator function is given by

$$C_{\text{dGUE}}(t) = 1 - \frac{1}{d^2} \sum_{F_z} \sum_{kl} |\langle k | \hat{U}_{F_z}(t) |l\rangle|^4. \quad (31)$$

This is closely related to the coherence generating power (CGP) of the time evolution operator [69].

## V. SUMMARY AND DISCUSSIONS

The central question concerning quantum chaos is how classically chaotic dynamics inform us about specific properties of quantum systems, e.g., the energy spectrum, nature of eigenstates, correlation functions, and, more recently, entanglement. Alternatively, what features of quantum systems arise since their classical description is chaotic? It is now well understood that if the quantum system has an obvious classical limit, then the dynamics of quantities like entanglement entropy and the OTOC are characterized by the corresponding classical Lyapunov exponents (see for example [38] and references therein). Recently, the study of OTOC and scrambling of quantum information as quantified by operator growth has witnessed a surge in interest. This is supplemented by the role of non-integrability, symmetries, and chaos in the above as well as in the study of thermalization and statistical aspects of many-body quantum systems. Our work is an attempt to explore operator scrambling and OTOCs and the role of symmetries and conserved quantities in the process. For this purpose, we have employed a model system of KCTs that is simple enough yet exhibits rich dynamics. Many-body quantum systems have an intimate connection with quantum chaos. There had been a significant push in understanding the issues involving thermalization, irreversibility, equilibration, and coherent backscattering and the effects of quantum interference in such systems. ETH offers a rich platform to understand several of these phenomena. However, one needs to be extra careful in attributing chaos and non-integrability to ETH, as recent studies have shown that even a classical LMG model displays ETH properties [70, 71]. In our work, we have considered the simplest many-body system, the kicked coupled top, which is rich enough to allow us to study these aspects. We have taken up this line of study and explored how information propagates with operator scrambling and how the incompatibility of two operators can quantify this with time.

We have numerically studied the OTOCs in the KCT model, which exhibits chaos in the classical limit and conserves the angular momentum along the  $z$ -axis. The conservation law enables us to partition the system into distinct invariant subspaces with constant magnetization. We first considered the

largest invariant subspace and examined the scrambling in the fully chaotic regime. We observed an excellent quantum-classical correspondence between the OTOC growth rate and the classical Lyapunov exponents. We then studied the mixed phase space OTOC dynamics with the help of Pervival's conjecture. By initializing the system in a random mixture of the chaotic Floquet states, we studied the OTOC growth and contrasted it with the maximally mixed state. The results indicate that the operators are more likely to get scrambled if the initial state is chosen from the chaotic sea. This is reflected both in the short-time as well as the long-time behavior. Subsequently, we extended our analysis to the entire KCT system, investigating OTOCs for two distinct choices of initial operators. We found that the scrambling behavior differs depending on the choice of initial operators. Furthermore, conservation laws have been observed to impede operator dynamics, regardless of the choice of the initial operators. We then showed that the OTOC averaged over the local GUE operators is related to the operator entanglement as observed recently [46]. Moreover, the OTOC is related to the coherence generating power for the diagonal Gaussian operators [69].

One of the central focuses in quantum information science is to simulate these systems on a quantum device and on the related issues involving quantifying the complexity of these simulations, benchmarking these simulations in the presence of errors, and exploring connections to quantum chaos in these systems. How is information scrambling related to the complexity of simulating many-body quantum systems [72]? We hope our study paves for the exploration of these intriguing directions.

## ACKNOWLEDGMENTS

We are grateful to Arul Lakshminarayan for useful discussions. This work was supported in part by grant number SRG/2019/001094/PMS from SERB and MHRD/DST grants SB20210807PHMHRD008128, SB20210854EEMHRD008074 and DST/ICPS/QuST/Theme-3/2019/Q69.

- 
- [1] Fritz Haake. Quantum signatures of chaos. In *Quantum Coherence in Mesoscopic Systems*, pages 583–595. Springer, 1991.
  - [2] Jayendra N Bandyopadhyay and Arul Lakshminarayan. Testing statistical bounds on entanglement using quantum chaos. *Physical review letters*, 89(6):060402, 2002.
  - [3] Jayendra N Bandyopadhyay and Arul Lakshminarayan. Entanglement production in coupled chaotic systems: Case of the kicked tops. *Physical Review E*, 69(1):016201, 2004.
  - [4] Juan Maldacena, Stephen H Shenker, and Douglas Stanford. A bound on chaos. *Journal of High Energy Physics*, 2016(8):106, 2016.
  - [5] Pavan Hosur, Xiao-Liang Qi, Daniel A Roberts, and Beni Yoshida. Chaos in quantum channels. *Journal of High Energy Physics*, 2016(2):4, 2016.
  - [6] AI Larkin and Yu N Ovchinnikov. Quasiclassical method in the theory of superconductivity. *Sov Phys JETP*, 28(6):1200–1205, 1969.
  - [7] Adam Nahum, Sagar Vijay, and Jeongwan Haah. Operator spreading in random unitary circuits. *Physical Review X*, 8(2):021014, 2018.
  - [8] CW Von Keyserlingk, Tibor Rakovszky, Frank Pollmann, and Shivaji Lal Sondhi. Operator hydrodynamics, otocs, and entanglement growth in systems without conservation laws. *Physical Review X*, 8(2):021013, 2018.
  - [9] Vedika Khemani, Ashvin Vishwanath, and David A Huse. Operator spreading and the emergence of dissipative hydrodynamics under unitary evolution with conservation laws. *Physical Review X*, 8(3):031057, 2018.

- [10] Tibor Rakovszky, Frank Pollmann, and CW von Keyserlingk. Diffusive hydrodynamics of out-of-time-ordered correlators with charge conservation. *Physical Review X*, 8(3):031058, 2018.
- [11] Cheng-Ju Lin and Olexei I Motrunich. Out-of-time-ordered correlators in a quantum ising chain. *Physical Review B*, 97(14):144304, 2018.
- [12] Akshay Seshadri, Vaibhav Madhok, and Arul Lakshminarayan. Tripartite mutual information, entanglement, and scrambling in permutation symmetric systems with an application to quantum chaos. *Physical Review E*, 98(5):052205, 2018.
- [13] Arul Lakshminarayan. Out-of-time-ordered correlator in the quantum baker's map and truncated unitary matrices. *Physical Review E*, 99(1):012201, 2019.
- [14] Stephen H Shenker and Douglas Stanford. Black holes and the butterfly effect. *Journal of High Energy Physics*, 2014(3):67, 2014.
- [15] Sanjay Moudgalya, Trithip Devakul, CW Von Keyserlingk, and SL Sondhi. Operator spreading in quantum maps. *Physical Review B*, 99(9):094312, 2019.
- [16] Igor L Aleiner, Lara Faoro, and Lev B Ioffe. Microscopic model of quantum butterfly effect: out-of-time-order correlators and traveling combustion waves. *Annals of Physics*, 375:378–406, 2016.
- [17] Ivan Kukuljan, Sašo Grozdanov, and Tomaž Prosen. Weak quantum chaos. *Physical Review B*, 96(6):060301, 2017.
- [18] Ruihua Fan, Pengfei Zhang, Huitao Shen, and Hui Zhai. Out-of-time-order correlation for many-body localization. *Science bulletin*, 62(10):707–711, 2017.
- [19] Yu Chen. Universal logarithmic scrambling in many body localization. *arXiv preprint arXiv:1608.02765*, 2016.
- [20] Brian Swingle and Debanjan Chowdhury. Slow scrambling in disordered quantum systems. *Physical Review B*, 95(6):060201, 2017.
- [21] Yichen Huang, Yong-Liang Zhang, and Xie Chen. Out-of-time-ordered correlators in many-body localized systems. *Annalen der Physik*, 529(7):1600318, 2017.
- [22] Sreeram Pg, Naga Dileep Varikuti, and Vaibhav Madhok. Exponential speedup in measuring out-of-time-ordered correlators and gate fidelity with a single bit of quantum information. *Physics Letters A*, 397:127257, 2021.
- [23] Daniel A Roberts, Douglas Stanford, and Leonard Susskind. Localized shocks. *Journal of High Energy Physics*, 2015(3):51, 2015.
- [24] Stephen H Shenker and Douglas Stanford. Multiple shocks. *Journal of High Energy Physics*, 2014(12):46, 2014.
- [25] Efim B Rozenbaum, Sriram Ganeshan, and Victor Galitski. Lyapunov exponent and out-of-time-ordered correlator's growth rate in a chaotic system. *Physical review letters*, 118(8):086801, 2017.
- [26] Ravi Prakash and Arul Lakshminarayan. Scrambling in strongly chaotic weakly coupled bipartite systems: Universality beyond the ehrenfest timescale. *Physical Review B*, 101(12):121108, 2020.
- [27] Rodolfo A Jalabert, Ignacio García-Mata, and Diego A Wisniacki. Semiclassical theory of out-of-time-order correlators for low-dimensional classically chaotic systems. *Physical Review E*, 98(6):062218, 2018.
- [28] Ignacio García-Mata, Marcos Saraceno, Rodolfo A Jalabert, Augusto J Roncaglia, and Diego A Wisniacki. Chaos signatures in the short and long time behavior of the out-of-time ordered correlator. *Physical review letters*, 121(21):210601, 2018.
- [29] Xiao Chen and Tianci Zhou. Operator scrambling and quantum chaos. *arXiv preprint arXiv:1804.08655*.
- [30] Felix M Haehl, R Loganayagam, Prithvi Narayan, and Mukund Rangamani. Classification of out-of-time-order correlators. *SciPost Phys*, 6(001):1701–02820.
- [31] Xiao Chen, Tianci Zhou, David A Huse, and Eduardo Fradkin. Out-of-time-order correlations in many-body localized and thermal phases. *Annalen der Physik*, 529(7):1600332.
- [32] Sivaprasad Omanakuttan and Arul Lakshminarayan. Out-of-time-ordered correlators and quantum walks. *Physical Review E*, 99(6):062128, 2019.
- [33] José Raúl González Alonso, Nicole Yunger Halpern, and Justin Dressel. Out-of-time-ordered-correlator quasiprobabilities robustly witness scrambling. *Physical review letters*, 122(4):040404, 2019.
- [34] Fausto Borgonovi, Felix M Izrailev, and Lea F Santos. Timescales in the quench dynamics of many-body quantum systems: Participation ratio versus out-of-time ordered correlator. *Physical Review E*, 99(5):052143, 2019.
- [35] Bin Yan, Lukasz Cincio, and Wojciech H Zurek. Information scrambling and loschmidt echo. *Physical review letters*, 124(16):160603, 2020.
- [36] Efim B Rozenbaum, Leonid A Bunimovich, and Victor Galitski. Early-time exponential instabilities in nonchaotic quantum systems. *Physical Review Letters*, 125(1):014101, 2020.
- [37] Efim B Rozenbaum, Sriram Ganeshan, and Victor Galitski. Universal level statistics of the out-of-time-ordered operator. *Physical Review B*, 100(3):035112, 2019.
- [38] Alessio Lerose and Silvia Pappalardi. Bridging entanglement dynamics and chaos in semiclassical systems. *Physical Review A*, 102(3):032404, 2020.
- [39] Koji Hashimoto, Kyoung-Bum Huh, Keun-Young Kim, and Ryota Watanabe. Exponential growth of out-of-time-order correlator without chaos: inverted harmonic oscillator. *Journal of High Energy Physics*, 2020(11):1–25, 2020.
- [40] Saúl Pilatowsky-Cameo, Jorge Chávez-Carlos, Miguel A Bastarrachea-Magnani, Pavel Štránský, Sergio Lerma-Hernández, Lea F Santos, and Jorge G Hirsch. Positive quantum lyapunov exponents in experimental systems with a regular classical limit. *Physical Review E*, 101(1):010202, 2020.
- [41] Silvia Pappalardi, Angelo Russomanno, Bojan Žunkovič, Fernando Iemini, Alessandro Silva, and Rosario Fazio. Scrambling and entanglement spreading in long-range spin chains. *Physical Review B*, 98(13):134303, 2018.
- [42] Quirin Hummel, Benjamin Geiger, Juan Diego Urbina, and Klaus Richter. Reversible quantum information spreading in many-body systems near criticality. *Physical review letters*, 123(16):160401, 2019.
- [43] Tianrui Xu, Thomas Scaffidi, and Xiangyu Cao. Does scrambling equal chaos? *Physical review letters*, 124(14):140602, 2020.
- [44] Chaitanya Murthy and Mark Srednicki. Bounds on chaos from the eigenstate thermalization hypothesis. *Physical review letters*, 123(23):230606, 2019.
- [45] Robert de Mello Koch, Jia-Hui Huang, Chen-Te Ma, and Hendrik JR Van Zyl. Spectral form factor as an otoc averaged over the heisenberg group. *Physics Letters B*, 795:183–187, 2019.
- [46] Georgios Styliaris, Namit Anand, and Paolo Zanardi. Information scrambling over bipartitions: Equilibration, entropy production, and typicality. *Physical Review Letters*, 126(3):030601, 2021.
- [47] Daniel A Roberts and Beni Yoshida. Chaos and complexity by design. *Journal of High Energy Physics*, 2017(4):1–64, 2017.
- [48] PG Sreeram, Vaibhav Madhok, and Arul Lakshminarayan. Out-of-time-ordered correlators and the loschmidt echo in the quan-

- tum kicked top: how low can we go? *Journal of Physics D: Applied Physics*, 54(27):274004, 2021.
- [49] Patrick Hayden and John Preskill. Black holes as mirrors: quantum information in random subsystems. *Journal of high energy physics*, 2007(09):120, 2007.
- [50] Collin M Trail, Vaibhav Madhok, and Ivan H Deutsch. Entanglement and the generation of random states in the quantum chaotic dynamics of kicked coupled tops. *Physical Review E*, 78(4):046211, 2008.
- [51] Giancarlo Benettin, Luigi Galgani, Antonio Giorgilli, and Jean-Marie Strelcyn. Lyapunov characteristic exponents for smooth dynamical systems and for hamiltonian systems; a method for computing all of them. part 1: Theory. *Meccanica*, 15(1):9–20, 1980.
- [52] V. Constantoudis and N. Theodorakopoulos. Lyapunov exponent, stretching numbers, and islands of stability of the kicked top. *Phys. Rev. E*, 56:5189–5194, Nov 1997.
- [53] Freeman J Dyson. The threefold way. algebraic structure of symmetry groups and ensembles in quantum mechanics. *Journal of Mathematical Physics*, 3(6):1199–1215, 1962.
- [54] Xiao Chen, Rahul M Nandkishore, and Andrew Lucas. Quantum butterfly effect in polarized floquet systems. *Physical Review B*, 101(6):064307, 2020.
- [55] Jonah Kudler-Flam, Ramanjit Sohal, and Laimei Nie. Information scrambling with conservation laws. *arXiv preprint arXiv:2107.04043*, 2021.
- [56] Gong Cheng and Brian Swingle. Scrambling with conservation law. *arXiv preprint arXiv:2103.07624*, 2021.
- [57] Vinitha Balachandran, Giuliano Benenti, Giulio Casati, and Dario Poletti. From the eigenstate thermalization hypothesis to algebraic relaxation of otocs in systems with conserved quantities. *Physical Review B*, 104(10), Sep 2021.
- [58] Jaš Bensa and Marko Žnidarič. Two-step phantom relaxation of out-of-time-ordered correlations in random circuits. *Physical Review Research*, 4(1):013228, 2022.
- [59] Pieter W Claeys and Austen Lamacraft. Maximum velocity quantum circuits. *Physical Review Research*, 2(3):033032, 2020.
- [60] IC Percival. Regular and irregular spectra. *Journal of Physics B: Atomic and Molecular Physics*, 6(9):L229, 1973.
- [61] T Gorin, HJ Korsch, and B Mirbach. Phase-space localization and level spacing distributions for a driven rotor with mixed regular/chaotic dynamics. *Chemical physics*, 217(2-3):145–153, 1997.
- [62] Paul A Miller and Sarben Sarkar. Signatures of chaos in the entanglement of two coupled quantum kicked tops. *Physical Review E*, 60(2):1542, 1999.
- [63] Shohini Ghose and Barry C Sanders. Entanglement dynamics in chaotic systems. *Physical Review A*, 70(6):062315, 2004.
- [64] Xiaoguang Wang, Shohini Ghose, Barry C Sanders, and Bambi Hu. Entanglement as a signature of quantum chaos. *Physical Review E*, 70(1):016217, 2004.
- [65] Shruti Dogra, Vaibhav Madhok, and Arul Lakshminarayan. Quantum signatures of chaos, thermalization, and tunneling in the exactly solvable few-body kicked top. *Physical Review E*, 99(6):062217, 2019.
- [66] Vaibhav Madhok, Vibhu Gupta, Denis-Alexandre Trottier, and Shohini Ghose. Signatures of chaos in the dynamics of quantum discord. *Physical Review E*, 91(3):032906, 2015.
- [67] Vaibhav Madhok, Carlos A Riofrío, Shohini Ghose, and Ivan H Deutsch. Information gain in tomography—a quantum signature of chaos. *Physical review letters*, 112(1):014102, 2014.
- [68] Vaibhav Madhok, Carlos A Riofrío, and Ivan H Deutsch. Characterizing and quantifying quantum chaos with quantum tomography. *Pramana*, 87(5):1–13, 2016.
- [69] Namit Anand, Georgios Styliaris, Meenu Kumari, and Paolo Zanardi. Quantum coherence as a signature of chaos. *Physical Review Research*, 3(2):023214, 2021.
- [70] Shane P Kelly, Eddy Timmermans, and S-W Tsai. Thermalization and its breakdown for a large nonlinear spin. *Physical Review A*, 102(5):052210, 2020.
- [71] MR Lambert, Shan-Wen Tsai, and Shane P Kelly. Quantum memory at an eigenstate phase transition in a weakly chaotic model. *arXiv preprint arXiv:2112.07631*, 2021.
- [72] Lukas M Sieberer, Tobias Olsacher, Andreas Elben, Markus Heyl, Philipp Hauke, Fritz Haake, and Peter Zoller. Digital quantum simulation, trotter errors, and quantum chaos of the kicked top. *npj Quantum Information*, 5(1):1–11, 2019.